Available online at www.sciencedirect.com
ScienceDirect
Trans. Nonferrous Met. Soc. China 32(2022) 285−295
Transactions of Nonferrous Metals Society of China
www.tnmsc.cn

Bearing mechanism and thickness optimization of ore roof in bauxite stope

Shao-wei MA[1,2], Jian-hua HU[1], Ya-guang QIN[1], Qi-fan REN[1], Dong-jie YANG[1]

1. School of Resources and Safety Engineering, Central South University, Changsha 410083, China;
2. CINF Engineering Co., Ltd., Changsha 410019, China

Received 3 November 2020; accepted 25 May 2021

Abstract: Based on the elastic thin plate theory, the main law of the ore roof failure was analyzed and the formula of the ore roof thickness was deduced. The results show that the tensile stress in the roof center accounts for the roof failure. According to the limit failure conditions of the point, the formula of the ore roof thickness was derived. Taking No.10 stope of a bauxite mine as an engineering case, the optimal thickness of the ore roof was 0.36 m. The safety factor was taken as 1.3, therefore the design thickness was 0.5 m. In the whole industrial test process, the dynamic alarm devices did not start the alarm and the ore roof was not damaged. Compared with other stopes under similar conditions, its thickness was reduced by 0.1−0.3 m. The recovery rate of the ore roof was increased by 16.7%−37.5%.
Key words: bauxite; claystone; ore roof; elastic thin plate; optimal thickness; engineering case

1 Introduction

The stability of a stope roof is very important for underground mining. For bauxite, because the direct roof is mostly unstable claystone, it is necessary to preserve the ore roof with a certain thickness to ensure the stability. Experientially, a thick ore roof leads to a stable stope but loses a large amount of ore. Therefore, to decrease the ore loss, it is necessary to determine the minimum thickness of the ore roof.

Many researchers have studied how to determine a safe roof thickness in mines. GAO et al [1] established a mathematical model to predict the safe thickness for a stope roof by finite element numerical simulation and multiple stepwise regression analysis methods. ZHANG et al [2] analyzed the safe thickness of a goaf roof by the beam theory, the load transfer intersection line theory and the thickness span ratio method. HU et al [3] deduced the theoretical formula of the minimum thickness of a stope roof by the bending and shear strength theory. LIN et al [4] applied the thickness reduction method to calculate the safe roof thickness in a goaf. ZHOU et al [5] established a nonlinear neural network model to predict the safe roof thickness by finite element numerical simulation. ZHANG et al [6] used the RFPA numerical simulation software to simulate the damage and collapse process of a goaf roof and analyzed the relationship between the safe thickness and the span. LI et al [7] analyzed the relationship between the safe thickness and the goaf span by the structural mechanical beam method and the numerical simulation method. WANG et al [8] proposed a comprehensive method to determine the safe thickness of a goaf roof based on the mechanical calculations and numerical simulation analyses. HE [9] studied the failure mode of the roof under tension and punching failure by Vlasov's thick plate theory and deduced the critical thickness of the roof.

XU et al [10] deduced the safe roof thickness formula under filling body by the cusp catastrophe model. ZHU et al [11] estimated the safe roof

Corresponding author: Jian-hua HU, Tel: +86-13787056402, E-mail: hujh21@csu.edu.cn
DOI: 10.1016/S1003-6326(22)65794-7

thickness by the structural mechanics. LAN et al [12] applied the genetic algorithm of the Pareto optimal solution set to the multi-objective optimization problem of the response surface model and obtained the optimal roof thickness. WU [13] used the material description incremental finite element method to obtain the regression equation between the safe roof thickness and the goaf span. ZHEN et al [14] used the strength reduction technology and the dichotomy principle to obtain the safe roof thickness of various span goafs. JIANG et al [15] established the relationship between the horizontal stress and the safe roof thickness by the structural stability theory and introduced the fracture tensor to establish the relationship between the goaf roof thickness and the rock mass fracture density. LUO et al [16] studied the minimum roof thickness by elastic mechanics. DIEDERICHS and KAISER [17] presented design charts based on the linearity limit for the unsupported stability of jointed rock beams and analyzed the critical span–thickness–modulus relationship. PLEASE et al [18] analyzed the roof failure mechanism by the beam theory and calculated the safe roof thickness. SOFIANOS [19] studied the mechanical behavior of a voussoir hard rock beam roof and deduced the minimum thickness of the voussoir rock beam. ALEJANO et al [20] used the UDEC numerical simulation software to analyze the safety and stability of a stope with different magnesite stope roofs (0.5−1.5 m in thickness). YIOUTA-MITRA and SOFIANOS [21] deduced the analytical formulas to evaluate, for any given geometry, the loading and mechanical parameters of a multijointed roof and its deflection and strain in terms of the extreme arch thickness. Therefore, numerical simulations, elastic−plastic theory, genetic algorithms, cusp catastrophe model, voussoir beam model and other methods were commonly used to study the roof stability and calculate the optimal roof thickness.

Elastic thin plate theory was used to study the bending deformation and internal force of thin plates under the load perpendicular to the plate plane or the joint action of vertical loads and plate plane loads [22]. The elastic thin plate theory has been widely used in stope structure analysis, e.g., the relationship between the roof stability and stope structural parameters [23], the relationship between the roof stress state and the stope width [24] as well as the safe roof thickness of the stope [25]. MA et al [26] deduced the formula of the optimum thickness of a stope intervening pillar by the elastic thin plate theory and cusp catastrophe theory. However, the constraints of the above elastic thin plate theory are all edge constraints. In the room pillar method, the support and constraint of the pillars for the roof are point constraints, and the pillars and ore roof are orebodies. In this work, a mechanical model of a rectangular elastic thin plate with a four-point fixed support was established and the formula for the optimal thickness of the ore roof was derived. The engineering practice in a bauxite stope verified the rationality of the calculation results.

2 Mechanical model of ore roof

2.1 Failure characteristics of ore roof

Bauxite deposits are usually layered and lenticular. The integrity of orebody is good, and its Proctor coefficient f can reach 8−12. The direct floor is ferruginous claystone, the direct roof is claystone, and the indirect roof is dolomite. The integrity of the dolomite is better than that of the ore body, and it can bear a larger exposed area, while claystone is mostly fragmented and broken into mud with water. In this condition, the conventional room and pillar mining method cannot support the roof even with high strength support. To safely and efficiently exploit this type of bauxite, an enhanced room and pillar mining method with reserved ore roofs is often adopted, as shown in Fig. 1.

According to the key strata theory, when there are multilayer hard rock layers in the overlying strata of the stope, the rock strata that play a decisive role in all or part of the rock mass activity are called the key strata [27,28]. Dolomite is the key strata since it allows larger exposure area than that of bauxite and claystone. As the main bearing body of overlying strata, dolomite will deform with mining activities but not collapse. Therefore, there are two main failure modes of the stope roof: one is that the stope collapses until the dolomite forms a flat roof because the claystone is thin, as shown in Fig. 2(a). The other one is that the stope collapses to the natural caving arch because the claystone is thick, as shown in Fig. 2(b). In summary, stope structure with unreasonable parameters results in

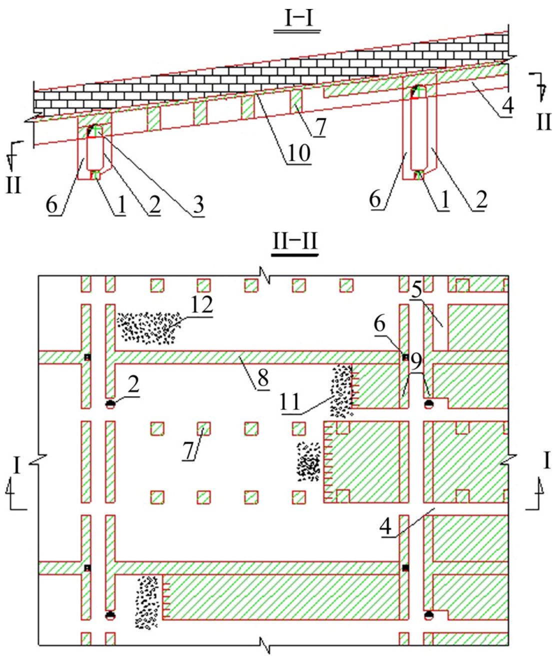

Fig. 1 Room and pillar mining method with reserved ore roof: 1−Transport drift; 2−Ore chute; 3−Connecting roadway; 4−Return airway; 5−Cutting drift; 6−Air intake shaft; 7−Pillar; 8−Intervening pillar; 9−Top and bottom pillar; 10−Ore roof; 11−Falling ore; 12−Waste rock

the instability of the stope, and the thickness of the ore roof is the primary structural parameter of the stope.

2.2 Mechanical analysis of ore roof

The structure of the ore roof is shown in Fig. 3, where t is the thickness of the ore roof, h is the thickness of the orebody, L is the length of the stope, d is the thickness of the claystone, W_p is the width of the point pillar, W_x and W_y are the widths between the two pillars in x- and y-direction, respectively, R_p is the radius of the plastic zone, and q is the uniform load of the ore roof. In underground engineering, the excavation of the rock mass will redistribute the stress in the rock mass. The ore roof is subjected to the pressure of the overlying strata, and the overlying strata gradually form small pressure-free arches. With the expansion of the goaf, the smaller pressure-free arches above the adjacent space gradually merge. A large non-pressure arch is formed, that is, a plastic zone with radius R_p above the goaf since the room and pillar are mined out and the whole stope gradually collapses.

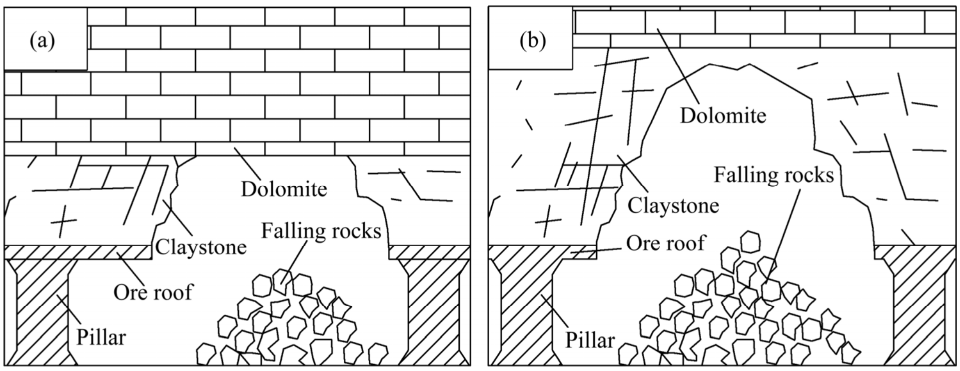

Fig. 2 Two failure modes of ore roof: (a) Flat structure; (b) Arch structure

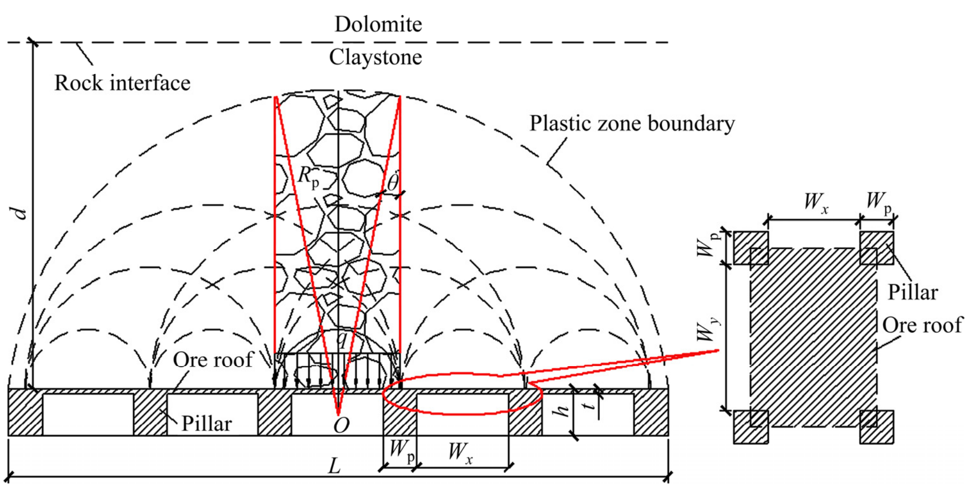

Fig. 3 Mechanical model of ore roof

Because the stability of dolomite is far greater than that of bauxite and claystone and the excavation disturbance of claystone is mostly a loose structure, the load borne by the ore roof is the self-weight of the claystone within the plastic zone above the roof. A reasonable ore roof can prevent the roof of the stope from falling, and improve the stress state and the overall stability of the stope.

According to the bearing mechanism, the load borne by the ore roof is the self-weight of all the rock masses within the plastic zone above the roof. Combined with the Protodyakonov's theory and the Kastner equation, the radius R_p of the plastic zone above the roof is [29]

$$R_\mathrm{p}=R_0\left[\frac{(P_0+c\cot\varphi)(1-\sin\varphi)}{c\cot\varphi}\right]^{\frac{1-\sin\varphi}{2\sin\varphi}} \tag{1}$$

$$R_0=\sqrt{(L/2)^2+(h/2)^2} \tag{2}$$

$$L=nW_\mathrm{p}+(n-1)W_x \tag{3}$$

$$P_0=\gamma H \tag{4}$$

where n is the number of point pillars, γ is the specific gravity of the overlying strata, H is the depth of the stope, c is the cohesive force, and φ is the internal friction angle of the rock in the plastic zone.

According to the stress situation of the ore roof, the ore roof in the middle of the stope is most likely to be damaged. Therefore, the ore roof in the middle of the stope was selected for mechanical analysis. In addition, due to the uneven thickness of the claystone, the uniform load of the ore roof is also different. According to the relationship between the radius of the plastic zone and the thickness of the claystone, the stress states is divided into the following two categories.

(1) When $d+h/2\geq R_\mathrm{p}$, a complete claystone free pressure arch plastic zone is formed.

(2) When $d+h/2<R_\mathrm{p}$, an incomplete claystone free pressure arch plastic zone is formed.

Therefore, the uniform load (q) of the ore roof can be calculated by the following formula:

$$q=\begin{cases}(R_\mathrm{p}-t)\gamma_\mathrm{c}+t\gamma_\mathrm{o},\ d+h/2\geq R_\mathrm{p}\\ d\gamma_\mathrm{c}+t\gamma_\mathrm{o},\ d+h/2<R_\mathrm{p}\end{cases} \tag{5}$$

where γ_c is the specific gravity of the claystone, and γ_o is the specific gravity of the ore.

2.3 Mechanical model of ore roof

After the stope is mined, the ore roof is regarded as a rectangular thin plate constrained by four-point pillars. The length and width of the rectangular roof are a and b ($b\leq a$, $a=W_x$, $b=W_y$), respectively, the elastic modulus is E, the Poisson's ratio is μ, the bending rigidity is D, the deflection of the plate is ω, and the roof stresses are σ_x, σ_y and τ_{xy}.

The boundary conditions of the elastic thin plate are as follows:

$$\begin{cases}(\omega)_{x=0,y=0}=0,\ (\omega)_{x=a,y=0}=0\\ (\omega)_{x=0,y=b}=0,\ (\omega)_{x=a,y=b}=0\\ \left(\dfrac{\partial\omega}{\partial x}\right)_{x=0,y=0}=0,\ \left(\dfrac{\partial\omega}{\partial x}\right)_{x=a,y=0}=0\\ \left(\dfrac{\partial\omega}{\partial x}\right)_{x=0,y=b}=0,\ \left(\dfrac{\partial\omega}{\partial x}\right)_{x=a,y=b}=0\\ \left(\dfrac{\partial\omega}{\partial y}\right)_{x=0,y=0}=0,\ \left(\dfrac{\partial\omega}{\partial y}\right)_{x=a,y=0}=0\\ \left(\dfrac{\partial\omega}{\partial y}\right)_{x=0,y=b}=0,\ \left(\dfrac{\partial\omega}{\partial y}\right)_{x=a,y=b}=0\end{cases} \tag{6}$$

The Rayleigh Ritz method was used to construct the deflection surface equation satisfying the boundary conditions:

$$\omega=A\left(a\sin\frac{\pi x}{a}+b\sin\frac{\pi y}{b}\right)^2 \tag{7}$$

where A is a set constant.

According to the thin plate bending theory, the total potential energy (V) of the ore roof was obtained without considering the strain component.

$$V=\frac{D}{2}\iint\left\{\begin{array}{l}\left(\dfrac{\partial^2\omega}{\partial x^2}+\dfrac{\partial^2\omega}{\partial y^2}\right)^2-\\ 2(1-\mu)\left[\begin{array}{l}\dfrac{\partial^2\omega}{\partial x^2}\dfrac{\partial^2\omega}{\partial y^2}-\\ \left(\dfrac{\partial^2\omega}{\partial x\partial y}\right)^2\end{array}\right]\end{array}\right\}\mathrm{d}x\mathrm{d}y-\iint q\omega\mathrm{d}x\mathrm{d}y \tag{8}$$

$$D=\frac{Et^3}{12(1-\mu^2)} \tag{9}$$

Substituting Eq. (7) into Eq. (8) yields

$$V=\frac{D\pi^4\left[\begin{array}{l}32ab^3(1+\mu)+32a^3b(1+\mu)+\\3\pi^2\left(a^4+b^4\right)+18a^2b^2\pi^2\end{array}\right]}{6ab}A^2-$$
$$abq\left[\frac{\left(a^2+b^2\right)}{2}+\frac{8ab}{\pi^2}\right]A \tag{10}$$

Given $\frac{\partial V}{\partial A}=0$, the following result was obtained:

$$A=\frac{3a^2b^2q\left[\pi^2\left(a^2+b^2\right)+16ab\right]}{4D\pi^6\left[\begin{array}{l}32ab^3(1+\mu)+32a^3b(1+\mu)+\\3\pi^2\left(a^4+b^4\right)+18a^2b^2\pi^2\end{array}\right]} \tag{11}$$

Then, ω can be expressed as

$$\omega=\frac{3a^2b^2q\left[\pi^2\left(a^2+b^2\right)+16ab\right]\left(\begin{array}{l}a\sin\frac{\pi x}{a}+\\b\sin\frac{\pi y}{b}\end{array}\right)^2}{4D\pi^6\left[\begin{array}{l}32ab^3(1+\mu)+32a^3b(1+\mu)+\\3\pi^2\left(a^4+b^4\right)+18a^2b^2\pi^2\end{array}\right]} \tag{12}$$

According to the stress derivation formula of elastic mechanics, the stresses of the ore roof are derived as

$$\sigma_x=-\frac{Et}{1-\mu^2}\left(\frac{\partial^2\omega}{\partial x^2}+\mu\frac{\partial^2\omega}{\partial y^2}\right)$$
$$=\frac{-2EtA\pi^2}{ab\left(1-\mu^2\right)}\left[\begin{array}{l}ab\left(\cos^2\frac{\pi x}{a}+\mu\cos^2\frac{\pi y}{b}\right)-\\\left(\begin{array}{l}a\mu\sin\frac{\pi y}{b}+\\b\sin\frac{\pi x}{a}\end{array}\right)\left(\begin{array}{l}a\sin\frac{\pi x}{a}+\\b\sin\frac{\pi y}{b}\end{array}\right)\end{array}\right] \tag{13}$$

$$\sigma_y=-\frac{Et}{1-\mu^2}\left(\frac{\partial^2\omega}{\partial y^2}+\mu\frac{\partial^2\omega}{\partial x^2}\right)$$
$$=\frac{-2EtA\pi^2}{ab\left(1-\mu^2\right)}\left[\begin{array}{l}ab\left(\mu\cos^2\frac{\pi x}{a}+\cos^2\frac{\pi y}{b}\right)-\\\left(\begin{array}{l}a\sin\frac{\pi y}{b}+\\b\mu\sin\frac{\pi x}{a}\end{array}\right)\left(\begin{array}{l}a\sin\frac{\pi x}{a}+\\b\sin\frac{\pi y}{b}\end{array}\right)\end{array}\right] \tag{14}$$

$$\tau_{xy}=-\frac{Et}{1+\mu}\frac{\partial^2\omega}{\partial x\partial y}=-\frac{2A\pi^2Et}{1+\mu}\cos\frac{\pi x}{a}\cos\frac{\pi y}{b} \tag{15}$$

Equations (13)−(15) show that the uniform load q and the thickness of the ore roof t influence the stress in the x-, y-direction and the shear stress.

3 Analysis of stress component of ore roof

Take a case of the ore roof with a=7 m and b=6 m to be analyzed. The thicknesses of the ore roof are leveled in 0.50, 0.75, 1.00 and 1.50 m, and the stress distribution diagram is used to analyze the stress. According to the actual situation of the mine, the physical and mechanical parameters of the lithology are listed in Table 1.

Table 1 Physical and mechanical parameters of the lithology

Lithology	Density, ρ/(g·cm^{-3})	Elastic modulus/GPa	Cohesion, c/MPa
Dolomite	2.761	7.099	2.137
Claystone	2.398	0.730	0.682
Bauxite	2.782	6.443	1.318

Lithology	Internal friction angle, φ/(°)	Poisson's ratio
Dolomite	37.172	0.295
Claystone	35.179	0.35
Bauxite	36.335	0.257

3.1 x- and y-direction stress analysis

It can be seen from Fig. 4(a) that the x-direction stress of different roof thicknesses is symmetrical with respect to plane $x=a/2$ and plane $y=b/2$. With the increase in the roof thickness, the x-direction stress gradually decreases. The critical line of the positive and negative stresses is the same for different roof thicknesses. The maximum tensile and compressive stresses appear in the center of the roof and near the point pillar, respectively, which is the key factor in determining a reasonable roof thickness. It can be seen that the overall trend of the curved surface in Fig. 4(b) is similar to that in Fig. 4(a).

3.2 Shear stress analysis

Figure 4(c) shows that the shear stress of different roof thicknesses is centrosymmetrical with respect to the point ($x=a/2$, $y=b/2$, z=0). The shear stress gradually decreases with increasing the thickness of the roof. The critical line of the positive and negative stresses is the same for different roof thicknesses. The maximum values of the positive and negative shear stresses appear near the point pillars, which is the key factor in determining a reasonable roof thickness.

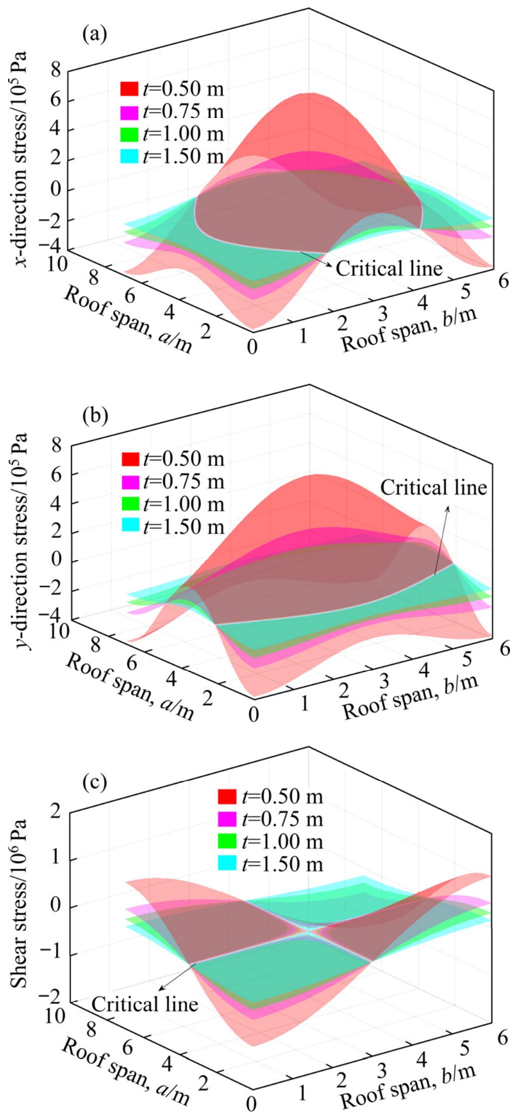

Fig. 4 Stress distribution diagrams of different roof thicknesses in x-direction (a), y-direction (b), and shear direction (c)

4 Stability analysis and thickness calculation of ore roof

4.1 Stability analysis of ore roof

The analysis of the roof stress demonstrates that the maximum value of the tensile stress and compressive stress appear in the roof center and near the point pillar respectively in Figs. 4(a) and (b). The shear stress in the center of the roof is 0, and the maximum values of the positive and negative shear stress appear near the point pillars. Different roof thicknesses lead to different stress conditions, a thin roof may lead to roof instability, while a thick roof may lead to resource waste. To avoid waste and fully recover mineral resources, the roof thickness should meet the following requirements:

$$\begin{cases} [\sigma_\mathrm{t}]\ge\sigma_x\big|_{x=\frac{a}{2},y=\frac{b}{2}},\ [\sigma_\mathrm{t}]\ge\sigma_y\big|_{x=\frac{a}{2},y=\frac{b}{2}} \\ -[\sigma_\mathrm{c}]\le\sigma_y\big|_{x=0,y=0},\ -[\sigma_\mathrm{c}]\le\sigma_x\big|_{x=0,y=0} \\ -[\tau_\mathrm{f}]\le\tau_{xy}\big|_{x=0,y=0},\ -[\tau_\mathrm{f}]\le\tau_{xy}\big|_{x=a,y=b} \\ [\tau_\mathrm{f}]\ge\tau_{xy}\big|_{x=a,y=0},\ [\tau_\mathrm{f}]\ge\tau_{xy}\big|_{x=0,y=b} \end{cases} \tag{16}$$

where σ_t is the tensile strength of the intact rock mass, τ_f is the shear strength of the intact rock mass, and σ_c is the compressive strength of the intact rock mass.

Through further analysis, the constraint conditions of the ore roof thickness are simplified as follows:

$$\begin{cases} [\sigma_\mathrm{t}]\ge\sigma_x\big|_{x=\frac{a}{2},y=\frac{b}{2}} \\ -[\sigma_\mathrm{c}]\le\sigma_y\big|_{x=0,y=0} \\ -[\tau_\mathrm{f}]\le\tau_{xy}\big|_{x=0,y=0} \end{cases} \tag{17}$$

The strength criterion of the Hoek-Brown rock mass [30,31]gives

$$\sigma_1=\sigma_3+\sqrt{m\sigma_3\sigma_\mathrm{c}+s\sigma_\mathrm{c}^2} \tag{18}$$

If σ_3=0, the uniaxial compressive strength of the rock mass is

$$\sigma_\mathrm{mc}=\sqrt{s}\sigma_\mathrm{c} \tag{19}$$

If σ_1=0, the uniaxial tensile strength of the rock mass is

$$\sigma_\mathrm{mt}=\frac{\sigma_\mathrm{c}}{2}\left(m-\sqrt{m^2+4s}\right) \tag{20}$$

$$\tau_\mathrm{f}=I\sigma_\mathrm{c}\left(\frac{\sigma}{\sigma_\mathrm{c}}-T\right)^J \tag{21}$$

where σ_1 and σ_3 denote the maximum and minimum principal stresses when the rock mass is destroyed, respectively, m is the Hoek-Brown constant, s is the quantity representing the quality dimension of the rock mass, σ_mc is the uniaxial compressive strength of the rock mass, σ_mt is the uniaxial tensile strength of the rock mass, σ is the normal stress of the rock mass, T is the parameter related to m and s, and I and J are constants which explain the relationship between the rock mass quality and the empirical constant [32].

The normal stress of the rock mass is

$$\sigma=\frac{1}{2}\sigma_{\mathrm{mc}}\left(1-\tan\varphi/\sqrt{1+\tan^2\varphi}\right) \tag{22}$$

Ore samples were taken from No.6, No.8 and No.10 stopes, and slightly processed with a geological hammer to form 3−5 cm square rock blocks. Ten to fifteen pieces were taken from each test site. The compressive strength of 108.92 MPa and tensile strength of 1.21 MPa were obtained by the point load data processing method.

According to the rock mass geological survey and referring to the relationship between the complete rock mass quality and the empirical constant, the Hoek Brown empirical constants are taken as m=6.9, s=0.052, φ=35°, I=0.427, J=0.683, and T=−0.004 [31]. According to Eqs. (19)−(21), the tensile strength, compressive strength and shear strength of the ore roof are 0.82, 24.83 and 2.41 MPa, respectively.

According to the constraint conditions (17), the $(\sigma_x-[\sigma_{\mathrm{mt}}])\big|_{x=\frac{a}{2},y=\frac{b}{2}}$, $-([\sigma_{\mathrm{mc}}]+\sigma_y)\big|_{x=0,y=0}$ and $-([\tau_{\mathrm{f}}]+\tau_{xy})\big|_{x=0,y=0}$ stress curves of different claystone thicknesses with increasing roof thickness were drawn. It can be seen from Fig. 5(a) that the $(\sigma_x-[\sigma_{\mathrm{mt}}])\big|_{x=\frac{a}{2},y=\frac{b}{2}}$ stress rapidly decreases with increasing roof thickness. The t value corresponding to $\sigma_x-[\sigma_{\mathrm{mt}}]=0\big|_{x=\frac{a}{2},y=\frac{b}{2}}$ is the minimum roof thickness ensuring the stope stable. Under the condition of a certain roof thickness, the $(\sigma_x-[\sigma_{\mathrm{mt}}])\big|_{x=\frac{a}{2},y=\frac{b}{2}}$ stress increases with increasing claystone thickness. In addition, the curve between the claystone thickness and the minimum roof thickness was plotted and the minimum roof thickness increases with increasing claystone thickness, as shown in Fig. 5.

The overall trend of the curve between Fig. 5(a) and Fig. 5(b) is similar, but when the roof thickness is 0.2 m, the $-([\sigma_{\mathrm{mc}}]+\sigma_y)\big|_{x=0,y=0}$ stress is still negative. According to the t−d curve in Fig. 5(b), when the claystone thickness is 50−60 m, the roof thickness for ensuring stope stability is less than

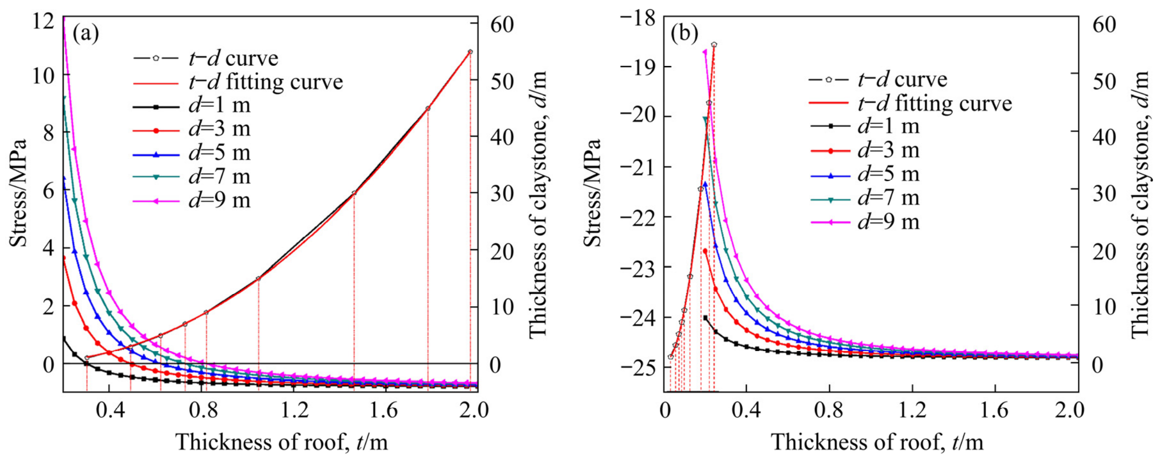

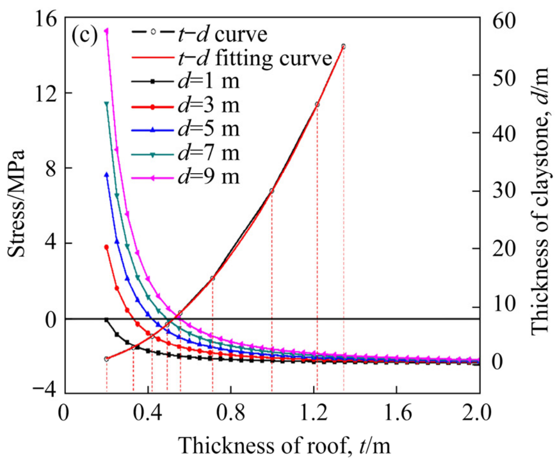

Figure No.	$d=it^j$	Value	Standard error	Adj.R-square
(a)	i	13.61556	0.05072	0.99997
	j	2.0673	0.00631	
(b)	i	942.07669	1.08379	1
	j	2.0082	0.00074085	
(c)	i	30.20734	0.03408	0.99999
	j	2.04567	0.00422	

Fig. 5 $(\sigma_x-[\sigma_{\mathrm{mt}}])\big|_{x=\frac{a}{2},y=\frac{b}{2}}$ (a), $-([\sigma_{\mathrm{mc}}]+\sigma_y)\big|_{x=0,y=0}$ (b), and $-([\tau_{\mathrm{f}}]+\tau_{xy})\big|_{x=0,y=0}$ (c) stress curves with increasing roof thickness under different claystone thicknesses

0.3 m, which shows that compressive stress does not cause roof instability.

It can be seen from Fig. 5(c) that the overall trend of the curve is similar to that in Fig. 5(a), and Fig. 5(a) needs a greater roof thickness than Fig. 5(c) to maintain stope stability under the same claystone thickness.

According to the analysis of Fig. 5, the condition for ensuring the stability of the roof protection mine is as follows:

$$[\sigma_{\mathrm{mt}}] \geq \frac{2EtA\pi^2}{ab(1-\mu^2)}(a\mu+b)(a+b) \tag{23}$$

$$t^2 \geq \frac{18abq\left[\pi^2(a^2+b^2)+16ab\right](a\mu+b)(a+b)}{\pi^4[\sigma_{\mathrm{mt}}]\begin{bmatrix}32ab(1+\mu)(a^2+b^2)+\\ 3\pi^2(a^4+b^4)+18a^2b^2\pi^2\end{bmatrix}} \tag{24}$$

If $B=\dfrac{18ab\left[\pi^2(a^2+b^2)+16ab\right](a\mu+b)(a+b)}{\pi^4[\sigma_{\mathrm{mt}}]\begin{bmatrix}32ab(1+\mu)(a^2+b^2)+\\ 3\pi^2(a^4+b^4)+18a^2b^2\pi^2\end{bmatrix}}$,

then,

$$t^2 \geq Bq \tag{25}$$

4.2 Calculation of roof thickness

According to Eqs. (5) and (25), it can be concluded that

$$\begin{cases} t^2 - B(\gamma_{\mathrm{o}}-\gamma_{\mathrm{c}})t - BR_{\mathrm{p}}\gamma_{\mathrm{o}} \geq 0,\ d+\dfrac{h}{2}\geq R_{\mathrm{p}} \\ t^2 - B\gamma_{\mathrm{o}}t - Bd\gamma_{\mathrm{c}} \geq 0,\ d+\dfrac{h}{2}< R_{\mathrm{p}} \end{cases} \tag{26}$$

$$t \geq \begin{cases} \dfrac{1}{2}\left[B(\gamma_{\mathrm{o}}-\gamma_{\mathrm{c}})+\sqrt{B^2(\gamma_{\mathrm{o}}-\gamma_{\mathrm{c}})^2+4BR_{\mathrm{p}}\gamma_{\mathrm{c}}}\right], \\ \quad d+\dfrac{h}{2}\geq R_{\mathrm{p}} \\ \dfrac{1}{2}\left[B\gamma_{\mathrm{o}}+\sqrt{B^2{\gamma_{\mathrm{o}}}^2+4Bd\gamma_{\mathrm{c}}}\right],\ d+\dfrac{h}{2}< R_{\mathrm{p}} \end{cases} \tag{27}$$

5 Engineering application

According to the recovery index requirements of underground mining of bauxite mines in China (see Table 2) and the technical requirements of the room and pillar mining method, the alumina to silica ratio (A/S) of the bauxite is approximately 8.5, the point pillars cannot be recovered, and the recovery rate of the intervening pillars is 40%. Therefore, the comprehensive loss rate of the point pillar and intervening pillar is 8%, and the maximum loss rate of the ore roof is 17%. According to the loss of the ore roof, the maximum thickness of the ore roof can be estimated.

Table 2 Recovery rate of bauxite underground mining under different A/S ratios

Ore body thickness/m	A/S≥10	A/S=10−5	A/S≤5
h≥5	88	80	75
5>h>2	80	75	72
h≤2	75	72	70

The maximum thickness of the ore roof under different A/S ratios and orebody thickness (h) values are plotted in Fig. 6 based on the data in Table 2. Therefore, the maximum allowable thickness of the ore roof can be determined under different A/S ratios and orebody thickness values. If the maximum thickness of the ore roof still cannot guarantee the stope stability, it is necessary to carry out supporting or reduce the stope span.

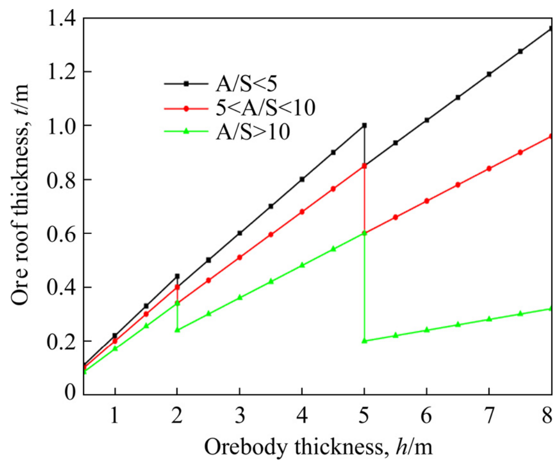

Fig. 6 Curves of maximum thickness of ore roof vs orebody thickness under different A/S ratios

The average thickness of the ore body in the NO.10 stope is 4.1 m. Its buried depth is about 250 m, the dip angle is about 8°, and the stope is about 50 m in width and 100 m in length. The strata structure of the uphill and drift in the No. 10 stope is detected by SSP GPR combined with drilling holes. Table 3 shows the measured results. To ensure the stope stability, the maximum thickness of the claystone is selected as 1.62 m.

Table 3 Measurement results of claystone thickness in No.10 stope

Location	Average thickness/m		Maximum thickness/m
	Drill	SSP	
Drift	1.22	1.15	1.42
No. 1 uphill	1.36	1.28	1.62
No. 2 uphill	1.19	1.23	1.49

The buried depth of No. 10 stope is 250 m. The average specific gravity, cohesive force and internal friction angle of overlying strata are 2700 kg/m^3, 0.682 MPa and 36.9° respectively. The number of point pillars is 6, the width of point pillar is 3 m, the spacing between point pillars is 6 m, and the average thickness of ore body is 4.1 m. According to Eqs. (1)−(4), R_p is 34.07 m. Because $d+h/2$ (3.67 m) is far less than R_p (34.07 m), the calculation formula for the roof thickness is as follows:

$$t=\frac{1}{2}\left[B\gamma_o+\sqrt{B^2\gamma_o^2+4Bd\gamma_o}\right] \tag{28}$$

Taking the parameters from Section 4.1, the solving optimal thickness of the ore roof was 0.36 m, the safety factor is 1.3, and the design thickness of the ore roof is 0.5 m. The roof dynamic alarm device is installed on the central roof of the four-point pillars in the stope. The alarm threshold of cumulative deformation and deformation rate of dynamic alarm device are set to be 20 mm and 5 mm/d, respectively, and the monitoring frequency is once per hour. In the whole stope mining process, the dynamic alarm device did not start the alarm, and the roof was not damaged. Compared with other stopes under similar conditions, the thickness of the ore roof in this stope was reduced by 0.1−0.3 m. The recovery rate of the ore roof was increased by 16.7%−37.5%.

Because the physical and mechanical parameters of the rock and stope structure parameters are basically the same, but the thickness of claystone is different (0−20 m). To simplify the calculation process of the roof thickness based on curve fitting, the calculation formula of the roof thickness is as follows:

$$t=\left(\frac{d}{13.616}\right)^{0.484} \tag{29}$$

$$d=13.616t^{2.067} \tag{30}$$

If the roof thickness exceeds a certain value, it will not meet the requirement of the recovery rate. Therefore, according to Fig. 6 and Eq. (30), the support distribution diagram under different A/S ratios, orebody thickness values and claystone thickness values can be drawn, as shown in Fig. 7.

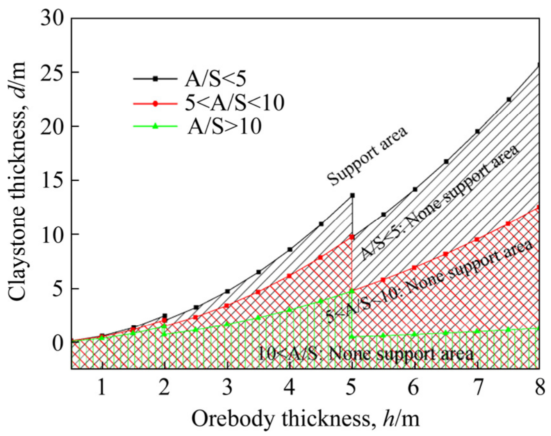

Fig. 7 Support distribution diagram under different A/S ratios, orebody thicknesses and claystone thicknesses

6 Conclusions

(1) The mechanical model of rectangular elastic thin plate with four points fixed support under different claystone thicknesses is established based on the elastic thin plate theory. The mechanical characteristics of bauxite ore roof structure are obtained, through the analysis of x-, y-direction stress and shear stress in different claystone thicknesses.

(2) Through the analysis of the stress concentration point and the most easily damaged point, it is found that the tensile stress in the center of the ore roof is the main reason for the roof failure. According to the limit failure conditions of the point, the formula of the ore roof thickness is derived.

(3) Taking the No. 10 stope of a bauxite mine as an engineering case, the optimal thickness of the ore roof is 0.36 m, and the design thickness is 0.5 m. In the whole stope mining process, the roof dynamic alarm device does not start the alarm, and the ore roof does not become damaged. The thickness of the ore roof in this stope is reduced by 0.1−0.3 m in comparison to 0.6−0.8 m thick ore roof under similar conditions in other stopes. The recovery rate of the ore roof is increased by 16.7%−37.5%. To simplify the stope management,

the support distribution diagram under different A/S ratios, orebody thickness values and claystone thickness values is drawn.

Acknowledgments

The authors are grateful for the financial support from the National Key Research and Development Program of China (No. 2017YFC0602901).

References

[1] GAO Feng, ZHOU Ke-ping, HU Jian-hua, DENG Hong-wei, TANG Gu-xiu. Mathematical forecasting model of safety thickness of roof for mining orebody under the complicated backfilling [J]. Geotechnical Mechanics, 2008(1): 177−181. (in Chinese)

[2] ZHANG Hai-bo, SONG Wei-dong, FU Jian-xin. Analysis of large-span goaf roof instability critical parameters and stability [J]. Journal of Mining and Safety Engineering, 2014, 31(1): 66−71. (in Chinese)

[3] HU Feng, LI Yun-an, LIU Hai-ao, ZOU Ji-tao, TAN Dao-yuan. Study of minimum safe thickness and ground subsidence deformation of the stope roof [J]. Metal Mine, 2013(8): 117−119, 123. (in Chinese)

[4] LIN Hang, CAO Ping, LI Jiang-teng, JIANG Xue-liang, HE Zhong-ming. The thickness reduction method in forecasting the critical safety roof thickness of gob area [J]. Journal of China Coal Society, 2009, 34(1): 53−57. (in Chinese)

[5] ZHOU Ke-ping, SU Jia-hong, GU De-sheng, SHI Xiu-zhi, XIANG Ren-jun. The nonlinear forecasting method of the least security coping thickness when mining under complex filling body [J]. Journal of Central South University (Natural Science), 2005(6): 1094−1099. (in Chinese)

[6] ZHANG Min-si, ZHU Wan-cheng, HOU Zhao-song, GUO Xiao-qing. Numerical simulation for determining the safe roof thickness and critical goaf span [J]. Journal of Mining and Safety Engineering, 2012, 29(4): 543−548. (in Chinese)

[7] LI Di-yuan, LI Xi-bing, ZHAO Guo-yan. Roof security thickness determination of underground goaf under open-pit mine [J]. Opencast Mining Technology, 2005(5): 21−24. (in Chinese)

[8] WANG Wei, LUO Zhou-quan, QI Fei-xiang, CAO Sheng-xiang. Safe roof blasting thickness of VCR stope under complex boundary condition [J]. Journal of Northeastern University (Natural Science), 2016, 37(5): 721−725. (in Chinese)

[9] HE Guang-ling. Determination of critical thickness of stiff roof in coal mine based on thick plate theory [J]. Chinese Journal of Underground Space and Engineering, 2009, 5(4): 659−663, 674. (in Chinese)

[10] XU Heng, WANG Yi-ming, WU Ai-xiang, LI Fang-fang, GAO Wei-hong. A computational model of safe thickness of roof under filling body based on cusp catastrophe theory [J]. Chinese Journal of Rock Mechanics and Engineering, 2017, 36(3): 579−586. (in Chinese)

[11] ZHU He-ling, ZHOU Ke-ping, XIAO Xiong, HU Jian-hua. Study on the minimum safety thickness of artificial roof based on reconstructing mining environment [J]. Mining and Metallurgical Engineering, 2008(1): 13−17. (in Chinese)

[12] LAN Ming, LIU Zhi-xiang, LI Xi-bing, LIU Qiang. Stope parameters optimization of level afterwards back-filling approach with medium-deep hole caving [J]. Journal of Central South University (Natural Science), 2018, 49(4): 933−939. (in Chinese)

[13] WU Wei-dong. Numerical simulation analysis of safe cover thickness of underground cavity [J]. Chinese Journal of Underground Space and Engineering, 2006(3): 449−452. (in Chinese)

[14] ZHEN Yun-jun, CHEN Kai-xiang, LIU Ying-fa, HU Jie. Determination of safe thickness of roof in underground goaf [J]. Industrial Minerals and Processing, 2007(9): 19−20, 36. (in Chinese)

[15] JIANG Xue-liang, CAO Ping, YANG Hui, LIN Hang. Effect of horizontal stress and rock crack density on roof safety thickness of underground area [J]. Journal of Central South University (Natural Science), 2009, 40(1): 211−216. (in Chinese)

[16] LUO Zhou-quan, XIE Cheng-yu, JIA Nan, YANG Biao, CHENG Gui-hai. Safe roof thickness and span of stope under complex filling body [J]. Journal of Central South University, 2013, 20(12): 3641−3647.

[17] DIEDERICHS M S, KAISER P K. Stability guidelines for excavations in laminated ground: The voussoir analogue revisited [J]. International Journal of Rock Mechanics and Mining Sciences, 1999, 36: 97−118.

[18] PLEASE C P, MASON D P, KHALIQUE C M, NGNOTCHOUYE J M T, HUTCHINSON A J, van der MERWE J N, YILMAZ H. Fracturing of an Euler–Bernoulli beam in coal mine pillar extraction [J]. International Journal of Rock Mechanics and Mining Sciences, 2013, 64: 132−138.

[19] SOFIANOS A I. Analysis and design of an underground hard rock voussoir beam roof [J]. International Journal of Rock Mechanics and Mining Sciences, 1996, 33(2): 153−166.

[20] ALEJANO L R, TABOADA J, GARCIA-BASTANTE F, RODRIGUEZ P. Multi-approach back-analysis of a roof bed collapse in a mining room excavated in stratified rock [J]. International Journal of Rock Mechanics and Mining Sciences. 2008, 45(6): 899−913.

[21] YIOUTA-MITRA P, SOFIANOS A I. Multi-jointed stratified hard rock roof analysis and design [J]. International Journal of Rock Mechanics and Mining Sciences, 2018, 106: 96−108.

[22] TIMOSHENKO S P. Theory of elastic stability [M]. 2nd ed. ZHANG Fu-fan, transl. Beijing: Science Press, 1965. (in Chinese)

[23] WANG Wei, LUO Zhou-quan, QIN Ya-guang, SUN Yang. Stope parameters optimization of non-pillar longhole retreat caving [J]. Journal of Northeastern University (Natural Science), 2016, 37(4): 578−582. (in Chinese)

[24] LUO Zhou-quan, WANG Wei, XIE Cheng-yu, JIA Nan, YAO Shu, YAN Ke-jun, CAO Sheng-xiang, XIANG Jun. Optimization of stope width of inclined medium thick ore body [J]. Journal of Central South University (Natural Science), 2015, 46(10): 3865−3871. (in Chinese)

[25] XIE Cheng-yu, LUO Zhou-quan, JIA Nan, YANG Biao, CHENG Gui-hai. Safety roof cutting thickness in mining gently inclined and extremely thick ore body [J]. Journal of Mining and Safety Engineering, 2013, 30(2): 278−284. (in Chinese)
[26] MA Shao-wei, LUO Zhou-quan, HU Jian-hua, REN Qi-fan, WEN Lei. Determination of intervening pillar thickness based on the cusp catastrophe model [J]. Advances in Civil Engineering, 2019, 2019(10): 1−11.
[27] QIAN Ming-gao, XU Jia-lin, MIAO Xie-xing. Green mining technology of coal mine [J]. Journal of China University of Mining and Technology, 2003(4): 5−10. (in Chinese)
[28] QIAN Ming-gao, MIAO Xie-xing, XU Jia-lin. Study on the theory of key strata in strata control [J]. Journal of China Coal Society, 1996(3): 2−7. (in Chinese)
[29] JI Wei-dong. Mining rock mechanics [M]. Beijing: Metallurgical Industry Press, 1991. (in Chinese)
[30] HE Jiang-da, ZHANG Jian-hai, FAN Jing-wei. Fracture analysis of *m*, *s* parameters in Hoek−Brown criteria [J]. Chinese Journal of Rock Mechanics and Engineering, 2001, 20(4): 432−435. (in Chinese)
[31] WANG Wen-xing. Rocks mechanics [M]. Changsha: Central South University Press, 2004. (in Chinese)
[32] HOEK E, BROWN E T. Practical estimates of rock mass strength [J]. International Journal of Rock Mechanics and Mining Sciences, 1997, 34(8): 1165−1186.

铝土矿采场矿石顶板承载机理与厚度优化

马少维 [1,2]，胡建华 [1]，秦亚光 [1]，任启帆 [1]，杨东杰 [1]

1. 中南大学 资源与安全工程学院，长沙 410083；
2. 长沙有色冶金设计研究院有限公司，长沙 410019

摘　要：基于弹性薄板理论，分析矿石顶板破坏的主要规律，推导矿石顶板的厚度求解公式。研究结果表明：矿石顶板中心的拉应力是矿石顶板破坏的主要原因，根据该点的极限破坏条件推导出矿石顶板的厚度求解公式；以某铝土矿第 10 采场为工程案例，经过求解，该采场最优矿石顶板厚度为 0.36 m，考虑安全系数为 1.3，设计矿石顶板厚度为 0.5 m；在整个工业试验过程中，顶板动态报警仪未启动报警，矿石顶板未发生破坏；相比类似条件的采场矿石顶板减少 0.1~0.3 m，矿石顶板回收率提高 16.7%~37.5%。

关键词：铝土矿；黏土岩；矿石顶板；弹性薄板；最优厚度；工程案例

(Edited by Xiang-qun LI)